Avalanche behavior in the draining of superfluid helium from the porous material Nuclepore

M. P. Lilly* and R. B. Hallock
Laboratory for Low Temperature Physics, Department of Physics, University of Massachusetts, Amherst, Massachusetts 01003
(Received 26 December 2000; published 19 June 2001)

Examination of the primary draining curve in studies of the capillary condensation of ^{4}He in the porous material Nuclepore reveals that lowering the chemical potential when the helium is in the superfluid state causes the Nuclepore pore spaces to drain in a series of large-scale avalanches in which substantial numbers of pores (up to ~2.5% of the sample) drain as a single cooperative event, i.e., as an avalanche. In this work we document the behavior of such avalanches in this porous material for two characteristic diameter pore sizes 200 nm and 30 nm. We examine the relevance of various theoretical models which one might apply to the system and conclude that none is completely satisfactory.

DOI: 10.1103/PhysRevB.64.024516 PACS number(s): 67.70.+n, 47.55.Mh, 67.40.Hf, 68.43.Mn

I. INTRODUCTION

The filling and draining of fluids from the pore spaces of porous materials is an area of study that has fundamental as well as practical value. Generally in such capillary condensation studies, measurements of filling and draining phenomena involve the measurement of the amount of fluid present in the adsorbing material as a function of the chemical potential of the fluid environment to which the adsorbing material is exposed. Such measurements typically reveal hysteresis with the filling and draining having a different functional dependence on the chemical potential. This difference can be related to the microscopic pore structure of the material, and such studies are valuable in the characterization of various porous materials. This information is useful in its own right, and it is of practical value to, for example, the chemical industry, oil recovery, and the soil sciences. Over the years a number of detailed studies have been conducted with a variety of adsorbed species. For example, studies of various porous substrates by Everett and his colleagues[1] using nitrogen, argon, and butane demonstrated the fundamental hysteresis behavior of these substrates and provided good examples of hysteresis subloops (hysteresis loops within hysteresis loops) and reversal curves (e.g., withdrawal of fluid prior to complete filling of the porous interior of the material).

In our work with hysteresis in porous materials, we have concentrated on a particularly interesting substrate, Nuclepore.[2] Nuclepore is a porous polycarbonate material with a planar geometry perforated by rather well-defined nearly cylindrical pores with a relatively narrow pore diameter distribution. We will describe this material further later in this work. Our working fluid is liquid helium—almost exclusively helium in the superfluid state. We have made this choice because superfluid helium is particularly pure and freely moves through porous materials in response to changes in the chemical potential. The use of such an inviscid fluid removes conceptual questions that can arise when removing viscous fluid from the porous material under study. We have previously reported hysteresis measurements of ^{4}He in Nuclepore.[3–6] Using superfluid ^{4}He as the working fluid does not affect the macroscopic hysteretic capillary condensation in any fundamental way, but the presence of the superfluid may affect the dynamics of pore draining and the mobility of the adsorbed film that coats the surfaces of the material.

In this previous work and in the work we report here, we have taken advantage of several of the properties of the superfluid to improve our measurements. As we will describe later, we use the properties of superfluid helium to provide an *in situ* measure of the chemical potential in the vicinity of our adsorbing material. This allows a precise measure of changes in the chemical potential close to saturated vapor pressure. In addition, the absence of viscosity and consequent mobility of the superfluid film allows rapid equilibration—the porous material readily tracks changes in chemical potential. In our studies of the hysteretic behavior of superfluid helium in Nuclepore we find that with an increase in chemical potential pore filling is a continuous process, but that for a decrease in the chemical potential, pore draining includes a series of significant avalanche events;[5] i.e., the draining behavior is not continuous. Such avalanche phenomena had not been seen previously.

The results of our observations of the avalanche behavior and our interpretations are the primary subjects of this report. Here we describe these measurements and the series of experiments which probed the properties of the capillary condensation avalanches. We will begin with a brief review of terminology and our technique.[6] Then, a series of results will be presented for both the 200 nm and 30 nm pore diameter Nuclepore. The avalanche event sizes, their location in the hysteresis loops, their duration, and many other features will be documented. In a subsequent paper,[7] we will describe a series of experiments[8] that were performed to gain further insight into the nature and cause of the avalanches. These show that *interactions* between and among the fluid reservoirs in the various pores lead to the cooperative phenomena of an avalanche.

II. TERMINOLOGY

Figure 1 serves to illustrate the terminology we will use. Here we show the fraction of the pores of a porous Nuclepore sample that are filled with the working fluid as a function of chemical potential. Such a global hysteresis loop results from a monotonic increase of the chemical potential

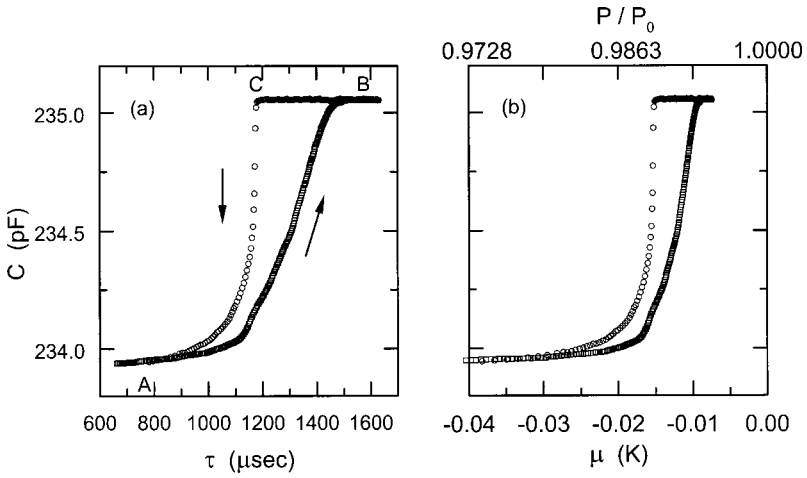

FIG. 1. A global hysteresis loop for 200-nm-pore-diameter Nuclepore showing the ascending locus and descending locus resulting from filling and draining for typical data. The amount of fluid condensed into the pores is measured by a capacitance technique described in the text. The data are shown as a function of (a) the third-sound time of flight and also in terms of (b) the chemical potential.

from the empty-pore state to the filled-pore state followed by a monotonic decrease to the empty-pore state. In practice, one accomplishes this by enclosing the porous material in a sample chamber in which one controls the chemical potential by controlling the temperature and the vapor pressure of the working fluid. The primary behavior seen for helium on Nuclepore is a gradual and smooth filling of the pores with increasing chemical potential (ascending locus) and a much more abrupt draining of the material over a relatively narrow range of chemical potential (descending locus). It is in this narrow range of rapid draining that we observe the avalanche events that are the subject of this report. We have investigated many of the properties of the hysteretic behavior of helium in Nuclepore and reported on it previously.[5,6] Here we will concentrate on the characterization of the avalanche behavior.

III. TECHNIQUE

As we reported previously,[6] to make hysteresis measurements on Nuclepore we utilized a capacitance technique[5] that is robust and relatively simple. With this we measure the amount of fluid contained in the pores of the material. The presence of *superfluid* liquid ^{4}He allows novel techniques to be used to measure the chemical potential in the system and enhances the temperature homogeneity of the sample. It also results in a rapid response of the fluid in the pores to changes in the chemical potential. To monitor the chemical potential *in situ* we use third sound.[9,10] Third sound is a surface-wave excitation on a superfluid helium film with a velocity that is a function of the chemical potential. Our third-sound detection scheme[5,6] involves thin-film aluminum superconducting thermometers and this limits the temperature range for studies that involve this technique to $1.3\ \mathrm{K} < T < 1.8\ \mathrm{K}$. In practice this is not a significant limitation.

The results reported here were obtained from a number of separate experiments. The temperature was regulated with an integrating temperature controller and drifts on the order of 1 mK were typical over the duration of the measurements. Three temperature sensors were mounted on the sample chamber: two carbon resistors—one to monitor the temperature and the other to regulate the temperature with electronic feedback—and a Lakeshore calibrated Ge thermometer[11] which provided a separate measure of the temperature.

The sample volume typically contained several adsorption substrates, each with a different purpose. One substrate was a single Nuclepore sheet on which the amount of ^{4}He in the pores was detected using the capacitive technique. A parallel plate capacitor was made by evaporating ≈ 50 nm of Ag on each side of each planar Nuclepore sample. The Ag film does not block the pore openings at the surface.[4,9] When ^{4}He liquid enters the pores, the dielectric constant (and therefore the capacitance) between the plates changes. The dielectric constant κ of ^{4}He is related to the atomic polarizability[12] by the Claussius-Mossitti equation[13]

$$\alpha = \frac{3V_m}{4\pi}\left(\frac{\kappa-1}{\kappa+2}\right), \tag{1}$$

where $\alpha = 0.1234\ \mathrm{cm}^3/\mathrm{mol}$ is the polarizability of ^{4}He and V_m is the molar volume. The capacitance was measured with an Andeen-Hagerling self-balancing capacitance bridge[14] that operated at 1000 Hz, and the measurements were recorded by a computer.

Given the relatively large size of the pores in Nuclepore, capillary condensation occurs very close to saturated vapor pressure, requiring a sensitive monitor of the chemical potential. As noted, the velocity of the third sound, a wave on superfluid ^{4}He films in which both the temperature and film thickness oscillate, provides such a monitor. We thermally generate a third-sound pulse on a flat borosilicate glass microscope slide in the sample volume by driving a current pulse of duration $W = 200\ \mu$sec through an Ag strip ($18\ \mathrm{mm} \times 0.15\ \mathrm{mm} \times 50$ nm) previously deposited on the glass surface by vacuum evaporation. The current pulse creates a third-sound wave with temperature amplitude ~ 200–$400\ \mu$K. The wave propagates along the length of the slide and the temperature fluctuation is detected with a current-biased Al thermometer ($18\ \mathrm{mm} \times 0.15\ \mathrm{mm} \times 30$ nm). Under typical operating conditions the thermometer has a sensitivity $dR/dT \approx 800\ \Omega/K$ when operated with a dc bias current $\approx 70\ \mu$A. The time of flight τ is readily found from the location of the intersection of the rising part of the received third-sound pulse and the extrapolated smooth base line that precedes the arrival of the pulse. With the measured time of flight of the pulse, τ, and the known

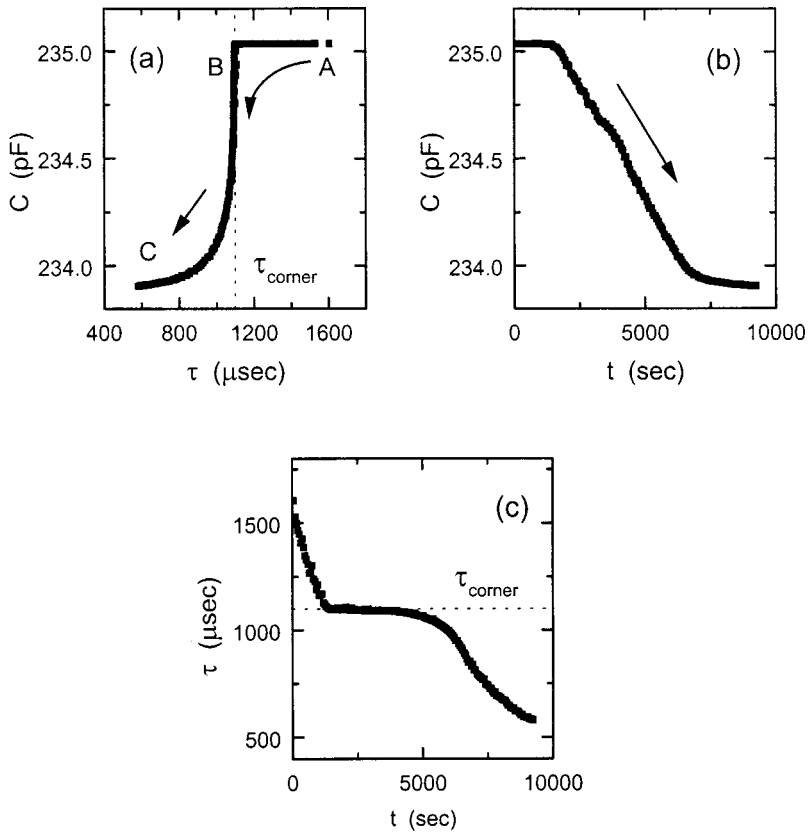

FIG. 2. Time dependence of the primary desorption curve for 200 nm Nuclepore. The results of measurements for the primary desorption curve, where C (our monitor of the filling fraction), τ and t are monitored, are shown for $T=1.441$ K. In this figure τ_{corner} denotes the value of the chemical potential at which pore draining begins in a significant way. In (a) we plot C vs τ for the case of draining. In (b) and (c) we plot the time dependence of C and τ for draining.

separation of the third-sound driver and detector, Δx, the velocity is $C_3=\Delta x/\tau$. The square of the superfluid velocity[15,16] is proportional to the superfluid fraction of the film (since only the superfluid moves) and to the restoring force due to the van der Waals interaction, and in this temperature range is given by

$$C_3^2=\left\langle\frac{\rho_s}{\rho}\right\rangle\left(1+\frac{TS}{L}\right)^2\frac{k_B\gamma\xi(3\gamma+4\xi)}{m_4 d^3(d+\xi)^2}, \tag{2}$$

where S is the entropy, L the latent heat, k_B Boltzmann's constant, m_4 the mass of ^{4}He, $\gamma=27$ layers^3 K, and $\xi=41.7$ layers.[17] The middle term represents a correction due to evaporation and condensation effects. The effective superfluid fraction $\langle\rho_s/\rho\rangle$ is slightly reduced from the bulk superfluid fraction ρ_s/ρ since the binding of ^{4}He is very strong close to the substrate, and is empirically given by

$$\left\langle\frac{\rho_s}{\rho}\right\rangle=\frac{\rho_s}{\rho}\left(1-\frac{a+bT(\rho/\rho_s)}{d}\right), \tag{3}$$

where the parameters for glass[18] are $a=0.5$ layers and $b=1.13$ layers/K. Using the measured C_3, Eq. (2) is numerically solved for the film thickness on glass, d. Finally,

$$\mu_{vdw,flat}=-\frac{\gamma\xi}{d^3(d+\xi)} \tag{4}$$

is used to determine the chemical potential in the sample chamber.

In all of the experiments described, ^{4}He gas was either added to or removed from the sample cell at a constant rate, equivalent to changing the adsorbed flat-surface helium film thickness at a rate of 0.5–2 monolayers/h. One monolayer of ^{4}He is taken to have a thickness of 0.36 nm. The adsorption results did not depend on the flow rate for these small values, and when the flow was stopped no relaxation effects were observed.

In typical operation we monitored the capacitance as a function of the measured third-sound time of flight. But this time-of-flight measurement required a finite interval of time and in some cases we made much more rapid measurements by simply measuring the capacitance of the draining Nuclepore sample as a function of time to obtain statistics on the avalanche behavior and to monitor the duration of an avalanche.

IV. AVALANCHES IN 200 nm NUCLEPORE

In Fig. 2(a), we plot the primary desorption curve for 200 nm Nuclepore at $T=1.441$ K as a function of the decreasing third-sound time of flight as ^{4}He is slowly removed from the experimental cell. As the ^{4}He removal takes place, the chemical potential is reduced and the third-sound time of flight is reduced (i.e., the third sound travels faster on a thinner film). At the value of the third-sound time of flight represented by τ_{corner} the draining of the pores begins. We plot C and τ as a function of time in (b) and (c), respectively. For hysteresis, our previous measurements showed that as long as the removal rate remains below a characteristic rate, ^{4}He can be removed at different rates, causing the time for com-

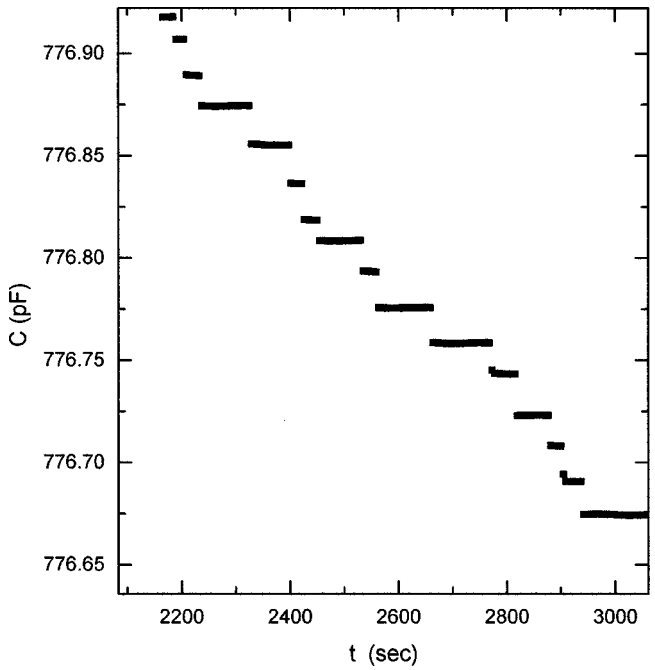

FIG. 3. An observation of avalanche behavior seen in the pumped-bath cryostat as pores drain in 200-nm-pore-diameter Nuclepore at $T=1.524$ K. The number of pores involved in an avalanche for a given jump in the capacitance illustrated is $\sim 2.5 \times 10^8$ pores/pF.

plete removal [in Figs. 2(b) and 2(c)] to change, but still reproducing the same primary desorption curve in (a). To learn how the pores drain for $\tau < \tau_{corner}$, the ideal way would be to take C and τ measurements very quickly (and accurately). In practice, for adequate precision each C measurement takes ~ 1.5 sec due to the internal averaging setting of the capacitance bridge, while each measurement of τ requires averaging of multiple (~ 1000) third-sound pulses. Collecting 1000 pulses and fitting the data to extract τ requires ~ 45 sec. To sample the primary desorption curve with a high data density we must either remove ^{4}He very, very slowly while monitoring both C and τ or measure C alone as a function of time t and remove ^{4}He at a more reasonable rate (but still more slowly than would show a noticeable effect on the hysteresis curves). There were a number of disadvantages to draining very slowly. First, the duration of draining was ultimately limited by the maximum time between helium transfers. Second, removing too slowly allowed the temperature fluctuations present in our apparatus to influence the behavior of the pore draining. Finally, the measurement of C was much more precise ($\delta C/C \sim 10^{-8}$) than the measurement of τ ($\delta\tau/\tau \sim 10^{-4}$). For these reasons we do not typically measure repetitively τ when studying avalanches, but typically only measure C vs t to determine the details of the behavior of the sample filling fraction during draining.

A. Measurements

Our first measurements to observe avalanches were carried out in a pumped-bath cyrostat. A typical observation of avalanches in the draining of hysteretic capillary condensated Nuclepore with 200-nm-diam pores is shown in Fig. 3. For this measurement ^{4}He was removed at a steady rate by pumping on the sample chamber through an impedance at room temperature. The capacitance of a 3.63-cm^2 capacitor formed on the Nuclepore was measured with the capacitance bridge set to average eight internal samples of duration 0.1 sec each. With the appropriate computer interfacing, the recorded capacitance data points were separated by ≈ 1.5 sec. When the entire draining is viewed, it appears relatively smooth, but structure is evident. Figure 3 is a magnified view of a small part of the draining. The capacitance drops in a series of steps separated by regions where the capacitance remains quite steady. We interpret these jumps in the capacitance as being due to groups or clusters of pores draining together in a time interval <1 sec. This is the avalanche phenomena that constitutes the primary subject of this report. Data obtained with the pumped-bath cryostat contained a number of apparatus induced artifacts. To resolve these problems a new cryostat with a continuously operating 1-K pot was constructed and we added a number of features to improve the stability of the system. With the new cryostat we had an increased time interval between helium transfers (~ 7 days), allowing more data to be collected without seriously disturbing the system. Finally, in all of the avalanche experiments we included ~ 200 sheets of 400 nm Nuclepore to serve as a helium film surface reservoir to help to stabilize the chemical potential. The presence of these larger-pore-size Nuclepore sheets was subsequently shown to have no influence on the hysteresis or avalanches observed in the 200-nm or 30-nm samples we studied.

To identify avalanches, we have used a number of criteria based on the capacitance steps seen in the data. These criteria are somewhat arbitrary, but work well until many of the pores have drained. First, to be considered an avalanche, the capacitance step has to have several stable points on either side of the step. This is the most striking aspect of the capacitance steps observed upon draining. While continuously removing ^{4}He, few pores empty for a time, and then suddenly a group of pores drains in $\lesssim 1$ sec. After the avalanche, there is another quiescent period when few pores drain. If the noise level were smaller than all of the avalanches, this would be the only condition needed. Since it is not, the size of the jump must be clearly out of the noise to be designated an avalanche. With this condition, we define a lower limit to the size of the observable avalanches below which we cannot unambiguously identify small jumps. If more than three data points are present in a capacitance step, we do not count this as a single avalanche. The reason for this condition is that we do not want to lump possible multiple avalanches into a single large event count. With these conditions it is relatively easy to count avalanches.

We estimate the approximate number of pores that are involved in an avalanche using the approximate pore density for Nuclepore, $\rho = 3 \times 10^8$ pores/cm^2, the area of the capacitors for the case just shown, $A = 3.63$ cm^2, the empty capacitance, $C_e = 772.8333$ pF, and the full capacitance, $C_f = 777.2747$ pF. For an avalanche of size ΔC, the fraction of the available pores that emptied is $\approx \Delta C/(C_f - C_e)$, neglect-

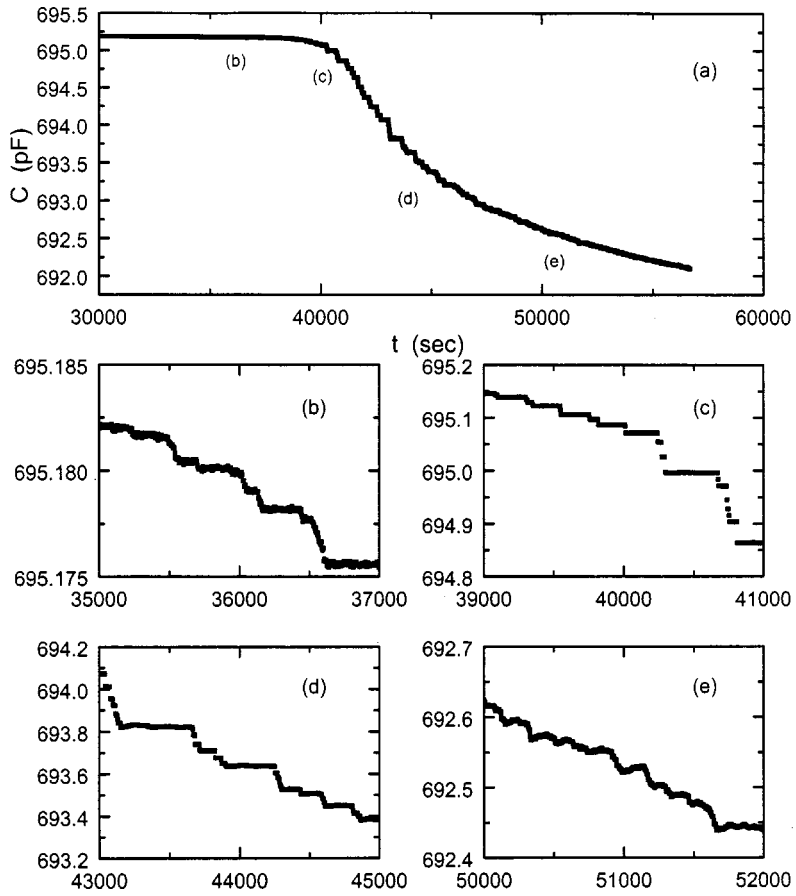

FIG. 4. Avalanches on Nuclepore with 200-nm pores at $T=1.476$ K taken using the 1-K-pot cryostat designed for improved stability. In views (b), (c), (d), and (e), various regions of the full draining data are expanded.

ing the film remaining on the surfaces of the empty pores (10% effect). The number of pores that drain is this fraction of the total number of pores between the capacitor plates,

$$N=A\rho\frac{\Delta C}{C_f-C_e}. \tag{5}$$

For this case, $N/\Delta C=2.45\times10^8$ pores/pF. This means the smallest resolvable avalanche involves $\sim5.9\times10^4$ pores, and the largest observed avalanche involves $\sim3.5\times10^7$ pores all draining in $\lesssim1$ sec. The duration of the avalanche events is an interesting question and we will return to it. For the data we have discussed so far, the time interval between measurements is ~1 sec, which implies that the avalanches have a duration no longer than ~1 sec.

In Fig. 4, we show a set of data for 200-nm-pore diameter Nuclepore taken at $T=1.476$ K. Further expanded views of various sections of the data shown in Figs. 4(b), 4(c), 4(d), and 4(e) are shown in Fig. 5. These avalanche data are typical of all of the data taken with the improved apparatus. Fluctuations in the capacitance that were due to the long-term manostat-induced temperature oscillations from the pumped-bath cryostat were eliminated. In Fig. 4(b) (notice the y axis only spans 0.01 pF), we show that very small avalanches were already visible before significant draining occurred. In this region [shown in Fig. 5(b)] the noise level is $\delta C=3\times10^{-4}$ pF. As the draining begins [$\mu\sim\mu_{corner}$, Fig. 4(c)] the size of the avalanches increases. The largest avalanches occur near the end of Fig. 4(c), and here $\delta C=1\times10^{-3}$ pF. As the draining proceeds, determining where the avalanches occurs becomes more difficult. By the time window shown in Fig. 4(e) and Fig. 5(e), $\delta C=3\times10^{-3}$ pF. While the noise floor on the capacitance signal was not improved significantly over the pumped-bath insert results, the long-term stability of the draining was improved, and small avalanches were visible that were not seen previously.

Using the criteria noted earlier, we identify 244 avalanches for the data in Fig. 4. The avalanche size versus filling plot is shown in Fig. 6 and reflects improved stability over that seen for the pumped-bath data. Avalanche sizes range over three orders of magnitude, with 10^{-4} pF$<\Delta C<10^{-1}$ pF. Using Eq. (5) for this data set, $N=2.47\times10^8$ pores/pF. Even though this capacitor has a different area (3.33 cm^2), the total change from empty to full is also different (4.037 pF), causing the sensitivity $N/\Delta C$ to be the same value as before. The number of pores that participate in the various avalanches are shown on the right axis of Fig. 6. There appear to be three regions of interest. In the first, in the arbitrary range 695.0 pF$<C<$695.2 pF or 0 pF$<C_{full}-C<0.2$ pF, avalanches begin as pores start to drain and the data obtained in this range contains 70 avalanches. Here the avalanches start very small and increase in size until the largest avalanches are observed. This initial region is shown in the inset in Fig. 6 (where the x axis is essentially reversed). The second region 694.0 pF$<C<$695.0 pF contains the largest avalanches observed during pore draining. These 18 avalanches accounted for 24.8% of the total fluid

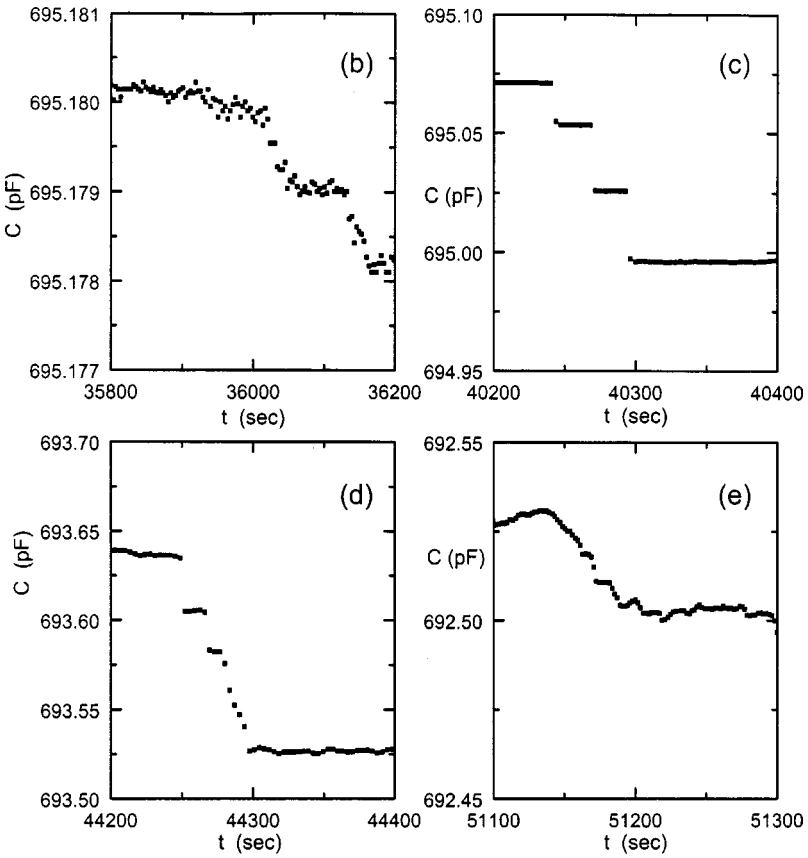

FIG. 5. Expanded view of avalanches on Nuclepore with 200-nm pores at $T=1.476$ K. For data from the entire data set, see Fig. 4.

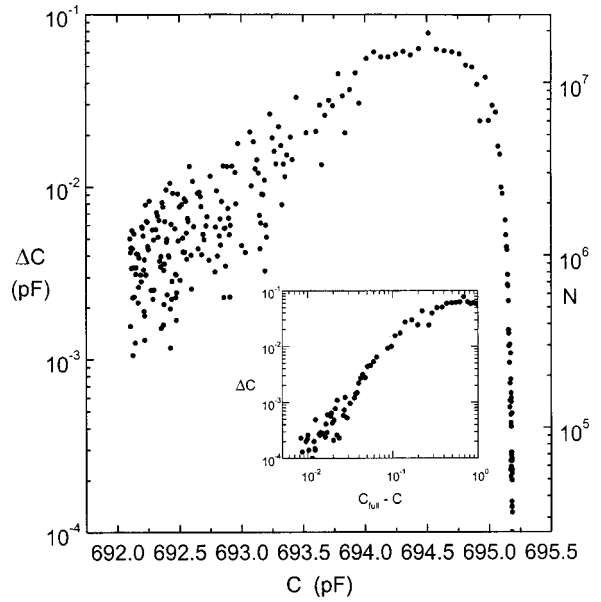

FIG. 6. Avalanche size ($s=\Delta C$) for the data shown in Fig. 4, $T=1.476$ K. The left axis shows the change in capacitance in an avalanche and the right side is an estimate of the number of pores involved in the avalanche. In the inset, we show an expanded view of the first avalanche that occurred by plotting $C_{full}-C$ on the bottom axis, where $C_{full}=695.1934$ (note that the *x* axis in the inset is flipped from that of the main figure).

drained. After the largest avalanches, the avalanche sizes begin to decrease. This decrease in overall size is accompanied by a spread in ΔC of about one-half an order of magnitude in size. Finally, when $C \lesssim 692.0$ pF ($\approx 80\%$ of the pore draining has occurred), any further avalanches in the system are indistinguishable from the noise in the capacitance measurement, δC.

Each of the avalanches shown in Fig. 4 has a size $s=\Delta C$, which we have shown as a function of the amount of ^{4}He in the pores in Fig. 6. To learn about the time interval between avalanches, we plot the avalanche size s as a function of the size of the time interval until the next avalanche Δt in Fig. 7. If a large avalanche caused the system to become more stable than a small avalanche, the data in Fig. 7 would be expected to show a trend of an increasing s with increasing Δt. The data show, somewhat unexpectedly, that this is not the case.

B. Statistics for 200 nm Nuclepore

Next, we define a size distribution function $D(s)$, where $s \equiv \Delta C$ and the probability of an avalanche with size between s and $s+ds$ is $D(s)ds$. In some systems with avalanches, the function $D(s)$ can display power law behavior.[19] A power law relation

$$D(s)=As^{\alpha} \tag{6}$$

indicates that there is no characteristic size scale in the region of the power law behavior. This can be compared to, for example, exponential behavior $D(s)=Be^{-s/s_0}$, where s_0 is a

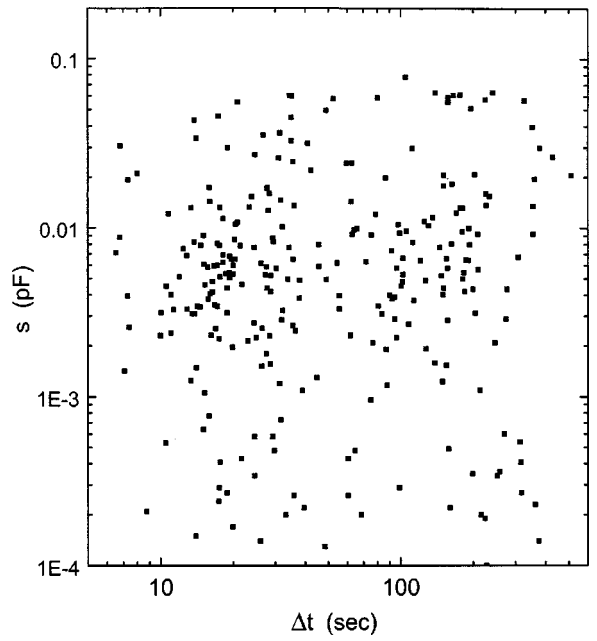

FIG. 7. The size ($s=\Delta C$) of a given avalanche vs the amount of time, Δt, between it and the next avalanche for 200-nm-pore-diameter Nuclepore at $T=1.458$ K. The data show that the time between avalanches did not depend on the size of the avalanche.

characteristic size scale. If two different systems can be characterized by the same power law for $D(s)$, these two systems are said to be in the same universality class.

In order to determine if $D(s)$ has a power law relationship with respect to avalanche size, we use a technique that requires no binning. For the particular set of avalanches of interest, the total number N^* of avalanches larger than size s is plotted as a function of s. If $N^* \sim s^m$ for a range of s, then a log-log plot of the data will, of course, result in a straight line in the range of power law behavior. To relate the exponent m, to the exponent α in Eq. (6) we use

$$N^* = \int_s^{s_{max}} D(s)ds = \frac{A}{\alpha+1}(s_{max}^{\alpha+1} - s^{\alpha+1}). \qquad (7)$$

If $N^* \sim s^m$ for $D(s) \sim s^\alpha$, then $\alpha = m-1$.

In Fig. 8, the results for several different sets of avalanche data are shown. Some experimental results obtained with the pumped-bath cryostat are shown in Fig. 8(a), while the rest of the data shown were taken using the 1-K-pot cryostat. In each panel, the solid squares represent all of the avalanches counted during the draining. The open circles shown in Figs. 8(b), 8(c), and 8(d) use only the initial avalanches (i.e., those that took place prior to the measurement of the maximum size avalanche in each data set). An example of the initial avalanches [Fig. 8(c), circles] are those with $C_{full} - C < 0.2$ pF, shown in the inset of Fig. 6. The reason that Fig. 8(a) did not have results for this initial avalanche region is because not enough avalanches were present to be recorded. In Fig. 9, we show the avalanche sizes for each of the data sets reported in Fig. 8.

The results for the statistics need to be considered with care. In some cases, as we see in Fig. 8(c) and Fig. 8(d), both

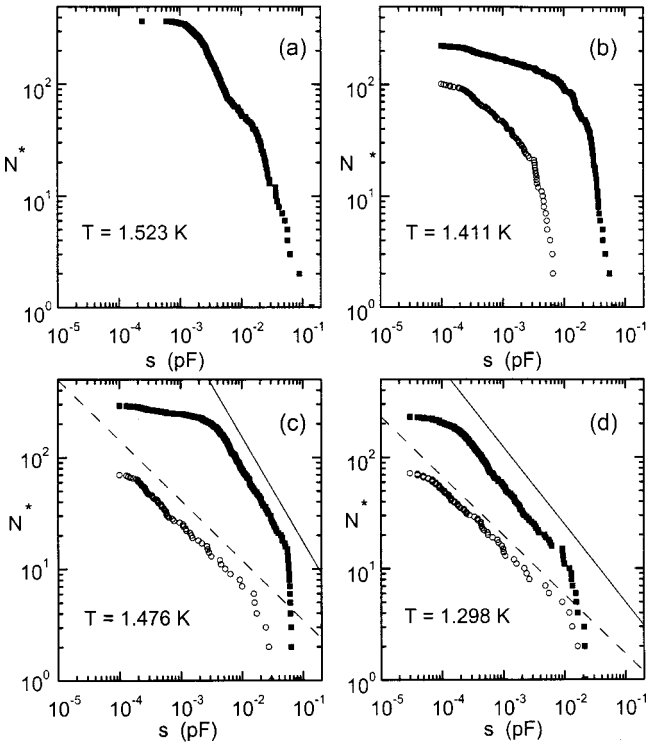

FIG. 8. Statistics for avalanches in the 200 nm Nuclepore. The total number N^* of avalanches larger than size s is plotted as a function of s. The solid squares include all of the avalanches counted. The open circles in (b), (c), and (d) include only the initial avalanches before the largest avalanche occurs in each case. The lines in (c) and (d) are lines with slopes reported in Table I. The solid lines fit all of the avalanche data; dashed lines fit the initial avalanche data prior to the occurrence of the maximum sized avalanche. These results are from several experiments with three different Nuclepore samples; in (b) and (c) the same sample was used.

the entire avalanche data set and the initial avalanches show apparent power law behavior. Such relatively clear power law behavior is not commonly observed. The initial regions appear consistent with each other, but the slopes of the entire data sets are not consistent. On the other hand, the more noisy results from the pumped-bath cyrostat [Fig. 8(a)] and also the results from one run with the 1-K-pot cryostat [Fig. 8(b)] do not show such clear power law behavior. The statistics for all of the other data sets we collected are similar to those shown in Fig. 8(a) and Fig. 8(b). One day separated the data runs shown in Fig. 8(b) and Fig. 8(c) and in one case the statistics obeys a power law while in the other they do not. While both had the same pumping (i.e., helium removal) rate, for the data of Fig. 8(b) the averaging setting resulted about 1.15 sec of averaging per data point, and for the data of Fig. 8(c) a longer averaging of about 2 sec was used. Based on our many observations, we doubt that the averaging time selected is significant. Table I summarizes the exponents for the straight lines shown in Fig. 8(c) and Fig. 8(d).

C. Comparison to theoretical models

Although the presence of power law behavior is not an unambiguous feature of the data, it is useful to compare these

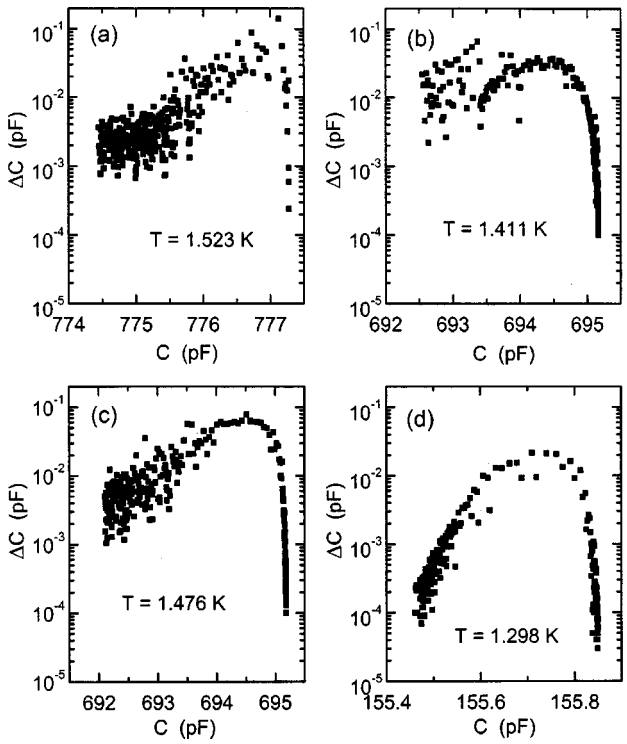

FIG. 9. Avalanche sizes for each experimental run shown in Fig. 8.

avalanche size distributions to the predictions of a number of models of avalanche behavior. The first theory we address is self-organized criticality (SOC).[20] Bak *et al.* proposed SOC as a very general model that would account for power law behavior in certain parameters (such as the power spectrum) for different systems without the need for a traditional second-order phase transition. In the ^{4}He/Nuclepore system, we may have present the basic features required. First, a parameter, the chemical potential, is slowly reduced. For a range of the chemical potential, this is somewhat analogous to slowly adding sand to a sandpile. Decreasing the chemical potential makes the system unstable, and an avalanche occurs. In experiments with sandpiles, avalanches increase the system stability. In our case as shown in Fig. 7, this is apparently not the case. For the two-dimensional sandpile, Bak *et al.* found $D(s) \sim s^{-1.0}$, different from our exponents, $-2 < \alpha < -1.5$. There are some qualitative differences between SOC and the ^{4}He/Nuclepore system. In SOC, avalanches of *any* size can occur at any time (limited by the system size). In Nuclepore, as seen in Fig. 6 sometimes only small avalanches will occur ($C \sim 695.2$ pF) and sometimes only large avalanches will occur ($C \sim 694.5$ pF). Furthermore, as ^{4}He is removed from the Nuclepore, more and more pores become empty. The configuration of filled pores changes and this can modify the avalanche behavior. In ideal SOC models, after an avalanche event, the sandpile still looks about the same, and the avalanches can continue as long as sand is added. This is not possible in the ^{4}He/Nuclepore system; removal of ^{4}He continuously changes the system and eventually all of the pores will be empty. Given these differences and our α values, we conclude that SOC is not likely to be a relevant model for the Nuclepore avalanches.

We next examine a model based on the random field Ising model (RFIM) discussed in detail by Sethna and co-workers.[21,22] In this model, Sethna *et al.* study a system of spins and find that avalanches occur, with the avalanche behavior dependent on the relative strength of the interaction between spins, J, and the strength of the random fields, R. When randomness dominates, $R/J \gg 1$, each spin acts independently and there are no avalanches. The limiting case of $R/J \to \infty$ is the Preisach model[23] of noninteracting spins. As R/J decreases, interactions cause spins to interact and to flip in groups (i.e., avalanches occur). The avalanche size distribution has power law behavior for small avalanches, but for large s, $D(s)$ is exponentially cut off. As R/J approaches a critical ratio ($R_c/J_c \sim 2.23$ in three dimensions), the cutoff is pushed to larger s. At R_c/J_c the avalanche size distribution shows a power law behavior. In the notation of Sethna *et al.*[21] the power law exponent is $\tau + \sigma\beta\delta$ if integrated over the entire external field and the exponent is τ if only a small portion of the external field is examined. When $R/J < R_c/J_c$, an infinite avalanche is present. An infinite avalanche is one that involves most of the spins in the system. For three dimensions, Sethna and co-workers find $\tau = 1.6$ and $\tau + \sigma\beta\delta = 2.03$ in simulations with systems of size 10^3 spins.

In the two-dimensional case of RFIM studied by Perkovic *et al.*,[22] the RFIM seems to show many orders of power law behavior before the exponential cut off appears even for R/J larger than the critical value. But the scaling forms are not well known. Fortunately, the exponents appear to be independent of the exact scaling form used.[22] For the two-dimensional case Perkovic *et al.* report values of $\tau = 3/2$ and $\tau + \sigma\beta\delta = 2$. Comparison between the RFIM model and our experimental results must be made with caution. Even if the RFIM holds for avalanches of superfluid He draining from Nuclepore, it is unknown how close the value of J/R in this system is to the critical J_c/R_c. Away from J_c/R_c, power law behavior is expected to be cut off. Due to the finite number of vertical intersections[6] among pores, Nuclepore presumably behaves as a two-dimensional network and should be compared with the two-dimensional case of the

TABLE I. Summary of exponents for the data in Fig. 8.

Figure	Curve	s range (pF)	m	α
8(c)	All (squares)	0.0044–0.050	-0.943 ± 0.002	-1.943
8(c)	Initial (circles)	1.9×10^{-4}–0.0156	-0.539 ± 0.004	-1.539
8(d)	All (squares)	2.4×10^{-4}–0.0119	-0.698 ± 0.003	-1.698
8(d)	Initial (circles)	7×10^{-5}–0.0119	-0.533 ± 0.004	-1.533

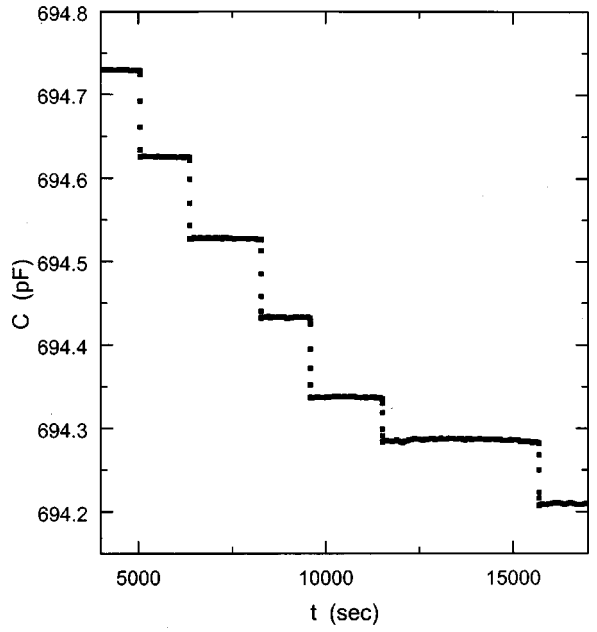

FIG. 10. Short-time-interval measurements reveal the duration of avalanche events on 200 nm Nuclepore at $T=1.475$ K for large avalanches. ^{4}He was removed through impedance $Z=1.5\times10^{10}$ cm^{-3} while measuring the capacitance every 0.27 sec.

RFIM. Because our measurements of scaling are made over a limited range of avalanche sizes, the slope of the lines in Fig. 8 may yield incorrect values for the power law predicted by the RFIM. Regardless, we compare $\tau+\sigma\beta\delta=2$ to the power law reported for the set of data including all of the avalanches, where we measure exponents of 1.94 and 1.70. The presence of the many small avalanches at the end of the avalanche sequence (Fig. 6, $C\lesssim693$ pF) strongly affects this exponent. The first value 1.94 is very close to 2, the value predicted by the RFIM. The second value is further from the prediction. A more consistent exponent for these two sets of avalanches is the power law that includes avalanches in the initial draining events [Fig. 9(c): $C>695.0$; Fig. 9(d): $C>155.75$ pF] where we found values of 1.54 and 1.53. Comparing this to the size distribution exponent $\tau=1.5$ for a narrow range of field (chemical potential) in the RFIM, the agreement appears to be rather good.

Our exponents are not inconsistent with those predicted by the RFIM. The question is, can the ^{4}He/Nuclepore avalanches be described by the RFIM? The RFIM consists of interacting elements in a random field. The randomness in Nuclepore is due to the complicated pore structure and the intersections between the pores. We can change this randomness by using a different realization of the porous material, i.e., by using a different pore size. Results for 30-nm-diam pores are reported later in this paper. The presence of RFIM behavior also requires the presence of an interaction between and among the elements of the system (i.e., the pores in our case). Extensive experiments probing the nature of pore-pore interactions that prove that such pore-pore interactions are present will be reported separately. So far, based on all of our work, we can only conclude that the RFIM *may* describe this system. The predictions of the RFIM are consistent with the exponents we observe in the cases where we see power law behavior.

Before ending this discussion on avalanche statistics, we discuss a final model that applies directly to capillary condensation systems. Guyer and McCall[24] have developed a capillary condensation model (CCM) with pore-pore interactions. This model demonstrates hysteresis due to these interactions even though the individual pores in the model are not hysteretic. In the CCM model, Guyer and McCall find that avalanches are present and that power law behavior may be expected in the avalanche size distribution.[25] The predicted exponents have not yet been reported. The origin of the interactions among the individual pores in Nuclepore is an interesting question. One source of these interactions is thought to be pore-pore intersections; the draining of one pore causes an intersecting pore to drain. Based on our results with more complicated Nuclepore substrate geometries[7,8] we have learned that the presence of *superfluid* ^{4}He enables a more complicated interaction between pores than simple direct pore-pore intersections, an interaction motivated by the presence of fluctuations in the superfluid helium film caused by pore draining. Guyer and McCall[26] have developed a separate model that is consistent with some of the experimental observations.

D. Additional measurements: Avalanche duration and measurements near T_λ

1. Avalanche duration

In order to measure the duration of the largest avalanches, we used a shorter averaging time with the capacitance bridge and at the same time increased the impedance[27] between the roughing pump and the sample cell, which resulted in a slower removal of helium from the sample cell. We only measured duration data for the largest of the avalanches. These results are shown in Fig. 10. A drawback of using a shorter averaging time is an increased amount of noise in the data. For the data shown in Fig. 10 the Andeen-Hagerling bridge was set so that the time between the measurement of the data points is $\Delta t\approx0.27$ sec, and between 3000 sec$\lesssim t\lesssim$16 000 sec, $\sim5\times10^4$ capacitance values were recorded. The results clearly show that the largest avalanches have a duration of about 1.3 sec, and the duration is clearly resolved.

The duration of 1.3 sec for the largest avalanches to occur is somewhat surprising. For an avalanche to occur, pores must drain in a cooperative event. For this to take place, some interaction must exist among the pores. To predict the duration of an avalanche event, we consider two effects: (1) the time required for a pore to drain and (2) the potential mechanisms of communication among the pores during pore draining. Pores ultimately must drain by the flow of helium film at the pore opening (ignoring evaporation). For a pore of length L and radius R, a volume of fluid of density ρ equal to $\pi R^2L\rho$ must drain by means of the flow of a film of thickness d moving no faster than a maximum velocity v_c. The time required for this is given by mass conservation, $2\pi Rd\rho_s v_s t=\pi R^2L\rho$, where we have assumed that one end

of the pore is slightly larger that the other and the pore drains through this end. If the two ends of a pore are precisely the same diameter, this may not be the case, and may lead to an overestimate of the time required to drain by a factor of 2. Thus, $t = RL\rho/2d\rho_s v_s \approx 10^{-4}/v_c$. If we assume[28] a value for the critical velocity $v_c \sim 0.2$ m/sec, then $t \sim 5\times10^{-4}$ sec is the time interval required for a single typical pore to drain. If some global event (e.g., vibration of the apparatus) were the cause of the avalanche event, one might expect that pores close the draining threshold would be simultaneously stimulated to drain and this would be a very rapid event. This is clearly not the case. A model for superfluid film motivated draining has been developed by Guyer and McCall.[26] This model predicts avalanche behavior stimulated by the leading and trailing edge of the excess fluid emitted onto the surface of the Nuclepore during a pore draining event.

Some form of communication leading to sequential stimulation must be present to cause the avalanche to require such an extended period of time. Two possibilities come to mind: (1) direct pore-pore interaction within the porous material or (2) the superfluid film that resides on the planar surfaces of the Nuclepore. The fluid that reaches the surface of the Nuclepore creates an increase in film thickness as a result of the draining of a pore. This can move across the surface as a disturbance, i.e., as a third-sound wave, at a speed $v_3 \sim 1.5$ m/sec for the temperature and film thickness ranges used in this work, resulting in a transit time for the sample (~ 2 cm) of ~ 1 msec. This estimate is for third sound on a smooth substrate. Index-of-refraction effects[3] will slow the propagation. Including index-of-refraction effects increases the time estimate to several msec. So if we were to imagine that a *single* pore were to stimulate an avalanche by the propagation of a *single* pore-draining-induced third-sound wave that spanned the Nuclepore surface, then the avalanche duration should be at most several msec rather than the ~ 1 sec that is observed. Our expectation upon seeing avalanches was that such a single-pore draining event might stimulate a prompt multipore avalanche. Such a model seems inconsistent with the data. Such a model is also perhaps problematic as the amplitude of third sound radiating outward will diminish quickly.

A modification of this model is the following. Presume that the draining of a single pore creates a third-sound wave that propagates locally and the avalanche event proceeds by a series of prompt pore draining events. A pore drains in $\sim 5\times10^{-4}$ sec. This is followed by a third-sound wave that stimulates a nearby pore to drain releasing another third-sound wave. With 5×10^6 pores involved in a typical avalanche event, such a pore is $\sim 10^{-3}$ cm away from a neighbor pore that will be stimulated to drain. Third sound reaches the neighbor pore in ~ 1 μsec following the initiation of the close-neighbor draining. So the typical pore-to-pore stimulation requires no more than $\sim 5\times10^{-4}$ sec. But all the pores must be reached. We can roughly estimate the time required by multiplying the number of pores likely to drain along, say, one edge of the measuring capacitor ($\sim 2.5\times10^3$), by the duration of a pore draining event ($\sim 5\times10^{-4}$ sec) yielding about 1.25 sec. This is reasonably close to the observed avalanche duration. Clearly the sequence of pore draining will not be a linear function of position across the sample; it will be more random, extending the time estimate somewhat. Thus, it appears as if the avalanches may involve the sequential draining of pores and this draining likely has a substantially ''in-series'' aspect. This brings up the possibility that one might be able to observe the spatial evolution of such avalanches as they progress across the substrate.

A final alternative is a model that requires direct pore-pore interactions in the material. Since the pores are filled and (for the case of 200-nm-pore-diameter Nuclepore) intersect each other an average of 5 times, the draining of one pore may perturb nearby pores. Consideration of this effect leads to a similar prediction for the duration of an avalanche event as pores that intersect sequentially drain. A rapid time-resolved measurement technique is required to establish conclusively whether such ''in-series'' effects are present.[29] An experiment with the proper geometry and with the time resolution to observe such behavior if it is present is under construction.

Finally, we should note that our observation of the presence of small avalanches suggests that pore-pore intersections may not be essential to the presence of avalanches. The small avalanches we observe involve a relatively small number of pores. If these are distributed across the sample (rather than being in a small cluster), they will be too far apart for direct pore-pore contact. We have demonstrated that this is indeed the case[8] and we will describe the details of these experiments more fully separately.[7] We are led to conclude that pore-pore intersections and the presence of the mobile helium film are both relevant to avalanche phenomena.

2. Temperature dependence

Another test of the avalanche behavior was to determine the effect of a substantial reduction in the superfluid density by changing the temperature. At temperatures $T > T_\lambda$, superfluid is no longer present. Without superfluid present, we expected that avalanches might not occur at all and perhaps the time constants associated with nonavalanche draining might change substantially. Unfortunately, due to the design of the 1-K pot and sample cell (designed for $T \sim 1.5$ K operation), the temperature regulation for $T \gtrsim T_\lambda$ was not adequately stable to look for avalanches. The highest temperature at which we were able to stabilize the temperature was $T = 2.061 \pm 0.001$ K. A hysteresis loop at this temperature was recorded by measuring the pressure of the sample cell with a 1000-torr Baratron gauge. This monitor of the chemical potential was necessary since the third-sound thermometers were no longer in the superconducting transition region (third sound would be extremely hard to see at this temperature in any event). The draining results for removing[30] ^{4}He at $T = 2.061$ K are shown in Fig. 11. This particular Nuclepore sample had a capacitor with an area of 0.98 cm^2. In the inset, the region shown for 234.8 pF$< C <$234.9 pF had the largest avalanches for experiments run at lower temperature. In Fig. 6, we see that the largest avalanches with a capacitor of area 3.33 cm^2 are ~ 0.1 pF. This should correspond to an avalanche of 0.029 pF for a capacitor of area 0.98 cm^2. Clearly no avalanches anywhere near this large occurred at $T = 2.061$ K. This avalanche run took less time than others

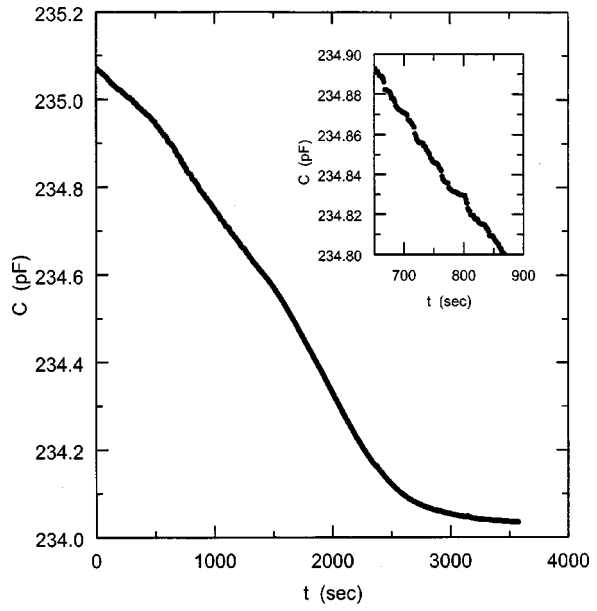

FIG. 11. Avalanche data for $T=2.061$ K. At this temperature the avalanche jumps either did not exist or were smaller than our experimental resolution.

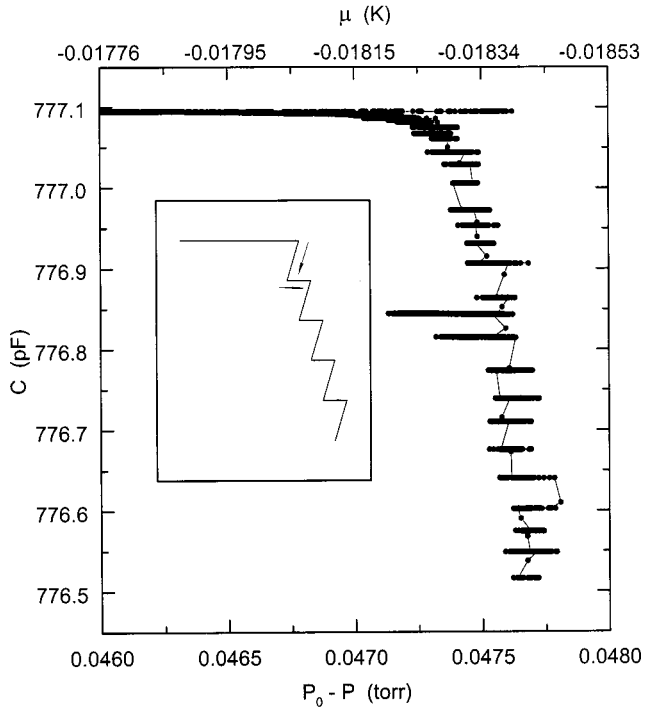

FIG. 12. Avalanches observed during helium removal while monitoring the chemical potential via the vapor pressure, P at $T=1.524$ K. The inset is a zigzag pattern that might be expected if the pressure in the sample cell increased after an avalanche, and then needed to be reduced before the next avalanche could occur. This is not observed in the data.

that we have measured. Here, the capacitance drops from 235.0 pF to 234.2 pF in ~ 2000 sec. Since $\Delta C=1.223$ pF, this means 66% of the volume drains in 2000 sec. For the data shown in Fig. 11, ^{4}He was removed about twice as quickly as in the case of the other measurements, but it is unlikely that this is the reason for the disappearance of avalanches. Such changes in the ^{4}He withdrawal rate at lower temperatures did not suppress avalanches. We conclude that as $T\rightarrow T_\lambda$, the avalanches either disappear or are extremely heavily suppressed. We will see a similar suppression for results in the presence of ^{3}He-^{4}He mixtures when we study the avalanche behavior of 30 nm Nuclepore.

3. Other measurement techniques

In our study of avalanche behavior we intentionally measured C vs t to minimize the time interval between measurements of the capacitance. As noted earlier, we used third-sound time of flight τ to monitor the chemical potential and relatively precise determinations of τ required tens of seconds. An alternate monitor of the chemical potential available whether third sound is present or not is the helium vapor pressure. Ideally this would be measured by means of an *in situ* pressure gauge, but one was not available to us during the course of this work. Instead we attempted to monitor the chemical potential externally by means of an mks Baratron pressure gauge.

The relationship between the pressure P and the chemical potential μ is $\mu=T\ln(P/P_0)$. A differential 10-torr Baratron head was used to measure P_0-P at room temperature at the top of the cryostat. One side of the differential gauge was connected to a small cell containing bulk ^{4}He adjacent to the sample cell, and the other side was connected directly to the sample cell. The results of C vs P_0-P are shown in Fig. 12 for an avalanche sequence at $T=1.524$ K and $P_0=3.9708$ torr. Equating the chemical potential of the film to the chemical potential of the vapor, we find (neglecting the retardation effect)

$$-\gamma/d^3\sim T\ln(P/P_0). \tag{8}$$

Since the pressure is very close to saturated vapor pressure, P_0-P is small. Expansion of Eq. (8) results in

$$P_0-P=\frac{\gamma P_0}{Td^3}. \tag{9}$$

We see that a larger value of P_0-P in Fig. 12 corresponds to a lower chemical potential and a smaller film thickness. The film thickness on glass can be found using Eq. (9) with $\gamma=27$ layers^3 K. The data is plotted with lines and symbols to show that avalanches do not always occur when P_0-P is at a maximum (avalanche occurrence at maximum values of P_0-P is shown schematically in the inset diagram). If a zigzag pattern such as shown in the inset were followed, we would conclude that after an avalanche, the pressure increased and the system needed to recover before another avalanche could occur. We do not observe this zigzag pattern, so if a pressure increase and subsequent recovery mechanism exists, the pressure changes are smaller than we could detect with the Baratron gauge.

The chemical potential for each value of P_0-P is plotted on the top axis with a nonlinear scale. There is a discrepancy between $\mu_{corner}=-0.014$ K observed with third-sound

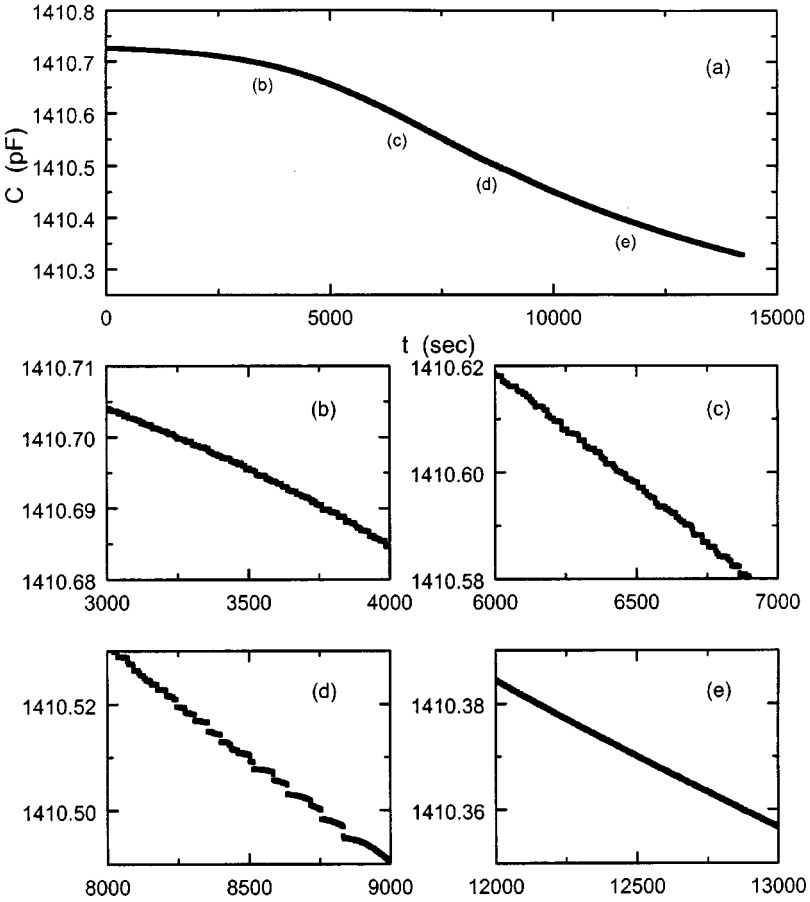

FIG. 13. Avalanches on Nuclepore with 30-nm-diameter pores for $T=1.436$ K.

measurements and $\mu_{corner}=-0.0183$ K observed with the differential gauge on the same run. One possibility that comes to mind is that the pressure measured at the top of the cryostat was not the same as the pressure in the experimental chambers due to the gravitational potential. The measured pressure P_m, a distance h above the sample cell, is related to P by $P_m=P\exp(-mgh/k_BT)$. Since the sample cell was immersed in a bath of ^{4}He at the same temperature, using $h\approx 1$ m results in $P_m=0.997P$. Since the saturated vapor pressure also has this factor, the net result including the gravitational potential is $\mu_{corner}=-0.018\,34$ K. The second possible reason for measuring a different pressure at the top of the probe is the thermomolecular effect. Due to collisions with the walls, the pressure measured at the warm end of a tube can be higher than the actual pressure at the cold end of the tube.[31] This effect is important when the mean free path of the ^{4}He atoms in the gas, L, is $\gtrsim$ the diameter of the tube. The mean free path of ^{4}He is

$$L=\frac{k_BT}{\sqrt{2}\pi d^2P}, \tag{10}$$

where $d=2.2$ Å for ^{4}He. At $T=1.524$ K and $P=3.97$ torr, we find $L=1.8\times10^{-5}$ cm. The tube radius was 0.25 cm, a much larger value. The small ratio $r/L=7.2\times10^{-5}$ indicates that the thermomolecular effect will not be important in this regime.

V. AVALANCHES IN 30 nm NUCLEPORE

Another set of avalanche experiments involved a smaller-pore-diameter Nuclepore. The original reason for using the smaller pore diameter was to change the connectivity of the pore spaces. As we learned from Nuclepore percolation simulations,[6] 200-nm-diam Nuclepore is connected well beyond the percolation threshold and each pore intersects an average of five other pores. The 30 nm Nuclepore, on the other hand, is made from the same material and has a similar pore structure, but due to the smaller pore diameter and reduced substrate thickness it is only at the threshold of percolation. The study of avalanches for the case of 30 nm Nuclepore allowed us to see similarities and differences between the two pore sizes. In addition to changing the connectivity, the primary draining curve for 30 nm Nuclepore occurred at lower values of and over a wider range of chemical potentials due to the smaller pore diameter and the apparent broader pore size distribution.

In Fig. 13(a), we show C vs t for the 30 nm Nuclepore as ^{4}He was removed. A closer view of the regions shown in Figs. 13(b), 13(c), 13(d), and 13(e) is shown in Fig. 14. When using the larger pore sizes, the avalanches occurred over a narrow range of μ, so ^{4}He was removed through an impedance at room temperature. For the smaller 30-nm pores, a faster ^{4}He removal rate was required because the primary draining curve covered a much broader range of μ. This faster removal was accomplished by removing ^{4}He

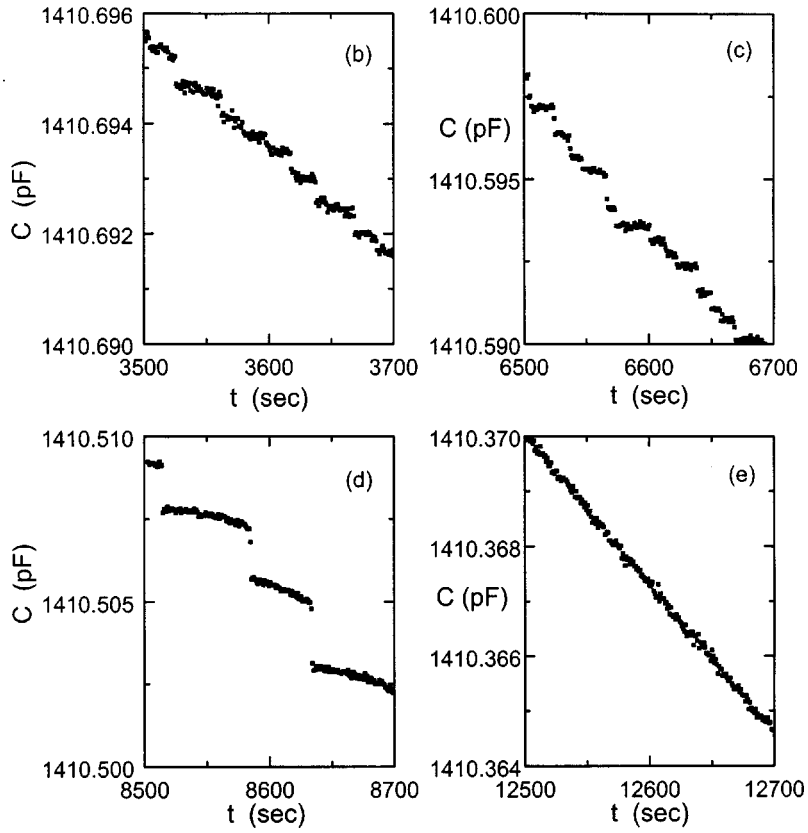

FIG. 14. Closer view of avalanches on Nuclepore with 30-nm-diam pores for $T=1.436$ K. The entire draining appears in Fig. 13(a).

through a needle valve (Nupro-B4JN). When the draining first begins, C drops smoothly without any avalanches being observed. The initial decrease in C is most likely due to effects of the compressibility[6,32] of ^{4}He, a larger effect at the lower chemical potentials where 30-nm-diam pores drain. When the pores are full, the noise is observed to be $\delta C \sim 10^{-4}$ pF. In Figs. 13(b), 13(c), 13(d), and 13(e), we magnify different regions along the draining data, and see that avalanches are present in Figs. 13(b), 13(c), and 13(d). These avalanches are very small at the start of draining, and as draining proceeds, larger avalanches become more likely. Not only are these avalanches easy to distinguish, the stability is improved and the data sets are much smoother than the earlier results for 200 nm Nuclepore. By the time $C=1410.50$ pF (filling fraction$=0.66$), the noise level, $\delta C \sim 5\times10^{-4}$, is lower than observed for 200-nm-pore-diameter Nuclepore ($\delta C \sim 1\times10^{-3}$ pF) at the same filling fraction. At this point, the largest size avalanches occur, after which C decreases continuously until the next large avalanche [see Fig. 14(d)]. This continuous draining is an indication of either pore-by-pore draining (no avalanches) or very many small avalanches each below our minimum resolution of 5×10^{-4} pF. At $C=1410.4970$ pF [Fig. 13(d)], the capacitance shows the largest step, and then no more avalanches are observed. After this largest avalanche, the capacitance drops continuously without any resolvable avalanches [Fig. 13(e) and Fig. 14(e)].

To measure the size of the avalanches, we use similar criteria to those described earlier. For the avalanches on 30-nm-pore-diameter Nuclepore, though, the noise is not as much of a factor in identifying avalanches. The criteria are simply that the size of the jump must be larger than 0.0002 pF (for the data in Fig. 13) and that the duration of the avalanche be less than 4 sec. The avalanche size range for the data in Fig. 13 at $T=1.436$ K is shown in Fig. 15. The size of the avalanche, ΔC, is plotted as a function C. Ava-

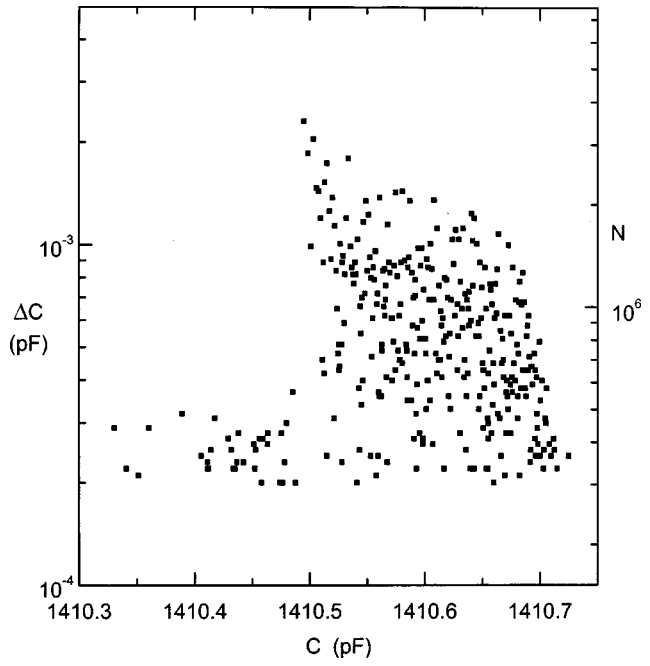

FIG. 15. Size of avalanche, s, vs capacitance for a complete draining of 30 nm Nuclepore for the data shown in Fig. 13, $T=1.436$ K.

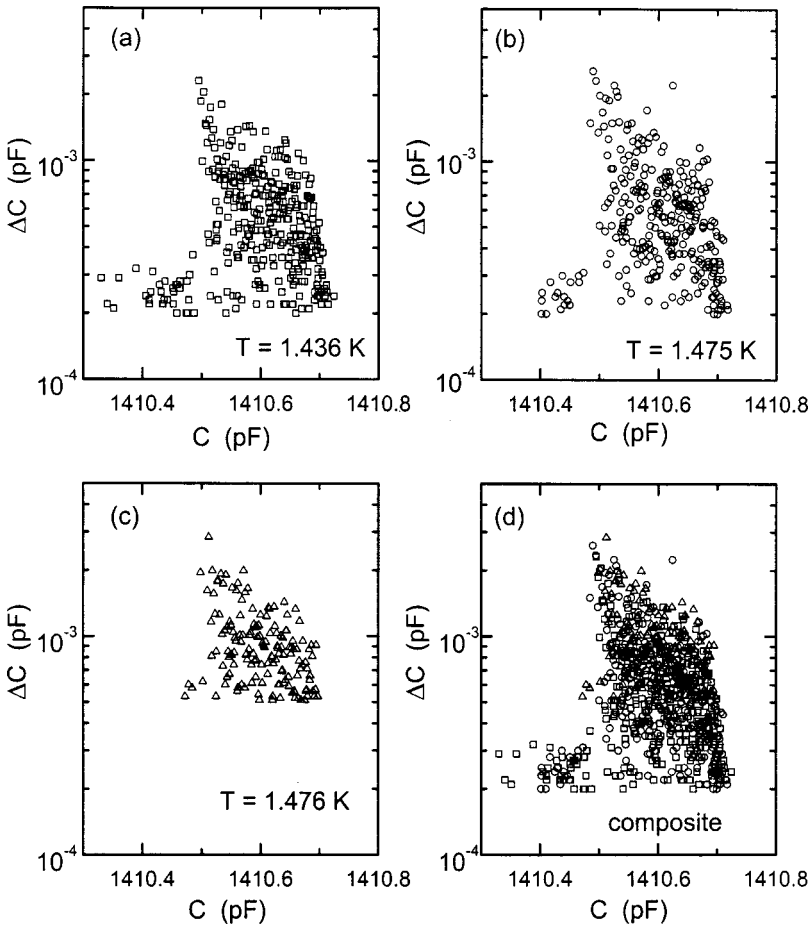

FIG. 16. Comparison of the avalanche sizes in 30 nm Nuclepore for three different removal rates and two different temperatures (see text). In (a) we show the data at $T=1.436$ K. In (b) we show the data at $T=1.475$ K. In (c) we show the data at $T=1.476$ K. The three are combined on the same plot in (d). All of these data are from the same 30-nm-pore-diameter Nuclepore sample.

lanches begin small and increase in size. As the pores drain, there is a distribution in the size of the avalanches; small avalanches can be seen at any time. This is different behavior from that seen for the avalanche size results for the 200 nm Nuclepore, where no small avalanches are observed when the largest avalanches occur (see Fig. 6). In the present case, the large avalanches for a given filling fraction define an envelope under which all avalanches fall. The size of the avalanches defining this envelope increases slightly as the draining continues. At $C=C_{cutoff}$, where $C_{cutoff} \simeq 1410.49$ pF, we see an avalanche cutoff after the largest avalanche (described above). Immediately above C_{cutoff}, the largest avalanches are observed. For all $C<C_{cutoff}$, we detect only a few jumps that are near the limit of resolution, δC.

Finally, with superfluid necessary for avalanches to continue to occur, we might speculate that the avalanche cutoff at $\simeq C=1410.49$ pF on 30 nm Nuclepore (Fig. 15) might be due to the Kosterlitz-Thouless (KT) transition on the Nuclepore. The KT transition occurred at $\mu \sim -0.50$ K on glass and the expected value of the KT transition on glass was $\mu_{c,glass}=-0.62$ K. Nuclepore is a different substrate, and will have a different critical film thickness (and chemical potential) for the KT transition. If the KT transition on Nuclepore occurred at a higher chemical potential than for glass, it is possible that the cutoff in the avalanches occurred because the ^{4}He film on the Nuclepore was no longer superfluid. The critical film thickness d_c at temperature T_c is

$$d_c=\frac{2k_BT_c}{\pi\rho_s}\left(\frac{m_4}{\hbar}\right)+D, \tag{11}$$

where ρ_s is the superfluid density and D the parameter from the effective superfluid fraction. Using $\rho_s/\rho=0.899$ and $\rho=0.1484$ g/cm^3 from Donnelly,[33] the first term evaluates to 1.07 layers at $T_c=1.476$ K. Using $D=a+bT\rho/\rho_s$, where $a=-0.25$ layers and $b=1.64$ layers/K,[9] the second term D is evaluated to 2.44 layers. The result is $d_c=3.52$ layers (on Nuclepore). The critical chemical potential is

$$\mu_c=-\frac{\alpha_N}{d_c^3}=-1.15 \text{ K}, \tag{12}$$

where $\alpha_N=50$ layers^3 K.[34] Since the KT transition occurs at a *lower* chemical potential than for glass, it is unlikely that this is the explanation for the cutoff in the avalanche sizes for the 30 nm Nuclepore sample shown in Fig. 15.

Since we were no longer removing ^{4}He through a fixed and well-defined impedance, the removal rate for removal via the needle valve was different for each of the several data sets collected. Several removal rates are present for the several different avalanche size plots, ΔC vs C, shown in Fig. 16. In this figure, the time for the Nuclepore to drain from 1410.7 pF to 1410.4 pF is 8234 sec [Fig. 16(a), squares],

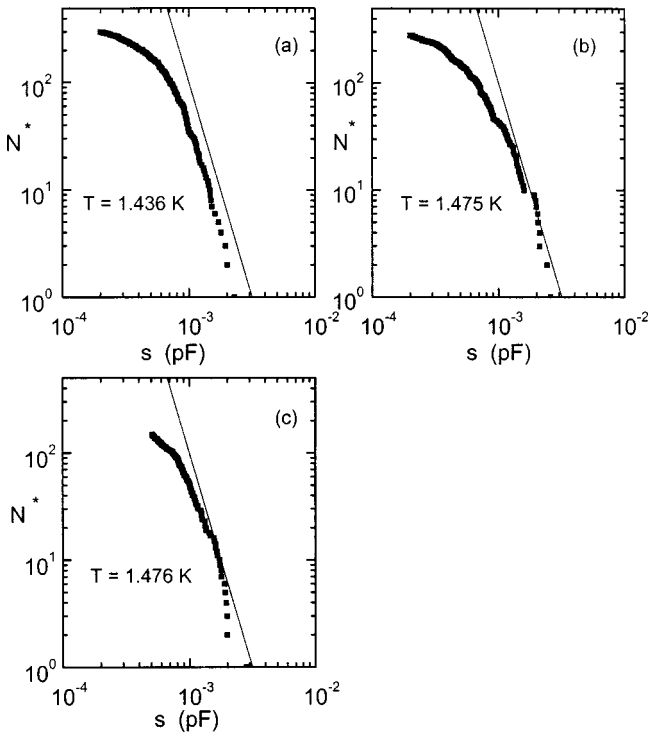

FIG. 17. Statistics for avalanches in 30 nm Nuclepore. For $C > C_{cutoff}$, $C_{cutoff} = 1410.48$ pF, the total number N^* of avalanches larger than size s is plotted as a function of s. The line $N^* = 10^{-10} s^{-4}$ is shown in (a), (b), and (c) for comparison. Unlike the 200 nm Nuclepore, due to the rather limited range of avalanche sizes present, there is no clear evidence for power law behavior.

9950 sec [Fig. 16(b), circles], and 1843 sec [Fig. 16(c), triangles]. Changing the rate did not significantly change the behavior of the avalanche size distributions, even for the case in which the rate was approximately 5 times faster than the other two drainings. Figure 16(d) is a composite of the three data sets. The envelope that defines the largest avalanches has the same shape for each of the runs, and for all three runs, C_{cutoff} occurs at about the same value. In each case the largest avalanches are observed just prior to cutoff. For the faster removal rate [Fig. 16(c), triangles], the resulting C vs t signal is more noisy causing an increased δC. Although the avalanches were not exactly reproducible, the different rates of ^{4}He removal do not seem to affect the size of avalanches.

A. Statistics for 30 nm Nuclepore

Next we compare the statistics for the avalanches observed in the case of 30 nm Nuclepore to those reported for the 200 nm Nuclepore. In Fig. 17, the total number of avalanches, N^*, larger than size s is plotted as a function of the avalanche size, s, for all of the avalanches that occurred for $C > C_{cutoff}$. All three of the avalanche data sets have similar behavior. In Figs. 17(a), 17(b), and 17(c) the line $N^* = 10^{-10} s^{-4}$ is shown for comparison. No conclusive evidence for power law behavior was observed, but in each case there was only a range in avalanche sizes of about 1 order of magnitude, $0.0002\ \text{pF} \leqslant \Delta C \leqslant 0.003$ pF (compared to ~ 3 orders of magnitude for the 200 nm Nuclepore).

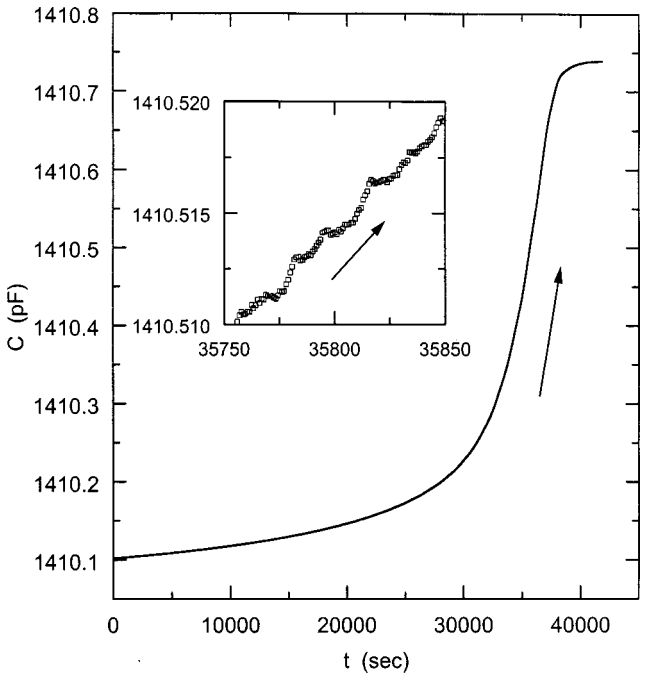

FIG. 18. Continuously adding ^{4}He to 30 nm Nuclepore at $T = 1.476$ K shows no sign of avalanches. The inset shows a magnified view of part of the data set.

B. Filling

Clearly, avalanches are present during the removal of ^{4}He from the Nuclepore. We looked for the possible presence of avalanches during the addition of ^{4}He using a 30-nm-pore-diameter Nuclepore sample. In Fig. 18, we show measurements of C while continuously increasing the chemical potential. In the inset is a magnification of part of this data set. Although the filling did not proceed completely uniformly, there are no identifiable sharp steps upon filling. This is consistent with our view of how filling must progress. The film thickness on the pores grows with an increase in chemical potential, and when individual pores fill, they do not significantly influence their neighbors. Our picture of pore draining is very different. Pores drain in groups (which are observed as avalanches) due to pore-pore interactions mediated by the pore-pore intersections, the geometry of those intersections, and/or by the role of the superfluid helium film that coats the parallel faces of the overall Nuclepore substrate. To reach conclusions about the nature of pore-pore interactions, a series of experiments has been performed designed to provide information on the spatial distribution of the avalanches and the mechanisms of pore-pore interactions. These experiments and the conclusions that they lead to have been reported briefly[8] and will be described in more detail in a forthcoming publication.[7]

C. Avalanches and ^{3}He-^{4}He mixtures

We carried out a set of experiments with ^{3}He-^{4}He mixtures to test the effect of using a ^{3}He-^{4}He mixture instead of superfluid ^{4}He in a further effort to determine how a reduction in the superfluid density might influence the avalanche

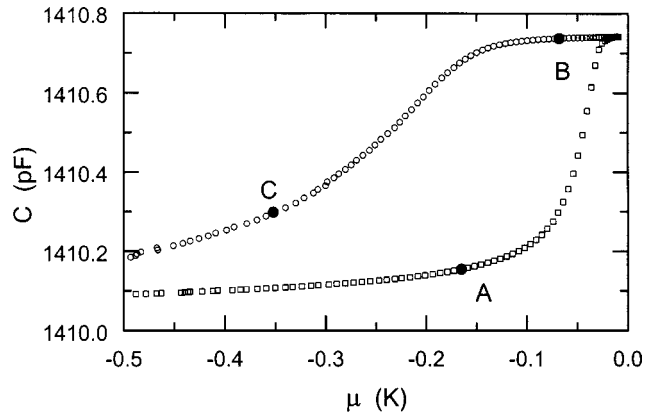

FIG. 19. Global hysteresis loop for 30 nm Nuclepore at $T=1.476$ K indicating where ^{3}He was added for the avalanche run with mixtures. At point *A*, the first addition of ^{3}He occurred. After filling with ^{4}He and partially draining the mixture, the second ^{3}He addition occurred at point *B*. From point *B* to *C* avalanches were recorded as helium was removed from the sample cell.

behavior. This was intended to complement our study in the vicinity of T_λ. We attempted this in spite of the fact that during removal of atoms from the sample cell the concentration in the cell would change due to the differential pumping rate for the two helium isotopes. The mixture was loaded into the sample chamber in two stages. Since we had been measuring avalanches and hysteresis loops for the 30-nm sample, ^{4}He was already in the sample chamber. The chemical potential was lowered by removing ^{4}He below the lower closure point of the global hysteresis loop for $T=1.476$ K. Figure 19 indicates where on the global hysteresis loop ^{3}He was added (points *A* and *B*) and where an avalanche sequence initiated near point *B* was halted (point *C*). First, ^{4}He was added to bring the system to point *A* in Fig. 19. A third-sound data set was taken. The purpose, to be described in more detail later, was to detect first sound in the vapor[35] and thus gain a measure of the ^{3}He concentration in the vapor. Before adding ^{3}He, the sample cell pressure measured with an mks Baratron at the top of the cryostat was $P=2.711$ torr. Here ^{3}He gas was admitted to the sample cell (point *A*), after which $P=4.508$ torr. Immediately after this addition, a second third-sound data set was recorded. The pores were then capillary condensed by adding ^{4}He. While adding, the capacitance was monitored and we determined that the presence of ^{3}He did not result in the presence of avalanches on filling (the same result as when adding ^{4}He, Fig. 18). After filling, the mixture was removed through a partially open valve by a roughing pump until $\tau=310$ μsec (point *B*, Fig. 19). At point *B*, a second addition of ^{3}He brought the pressure from $P=4.55$ torr to $P=7.65$ torr, but here no third-sound data set was taken. The mixture was again slowly removed through the partially opened valve while the capacitance was measured at a rapid sampling rate. At point *C*, the removal of the mixture was halted, and a final third-sound data set was recorded.

The results are shown in Fig. 20. When the mixture was slowly removed [Fig. 20(a)], the draining was smooth, with

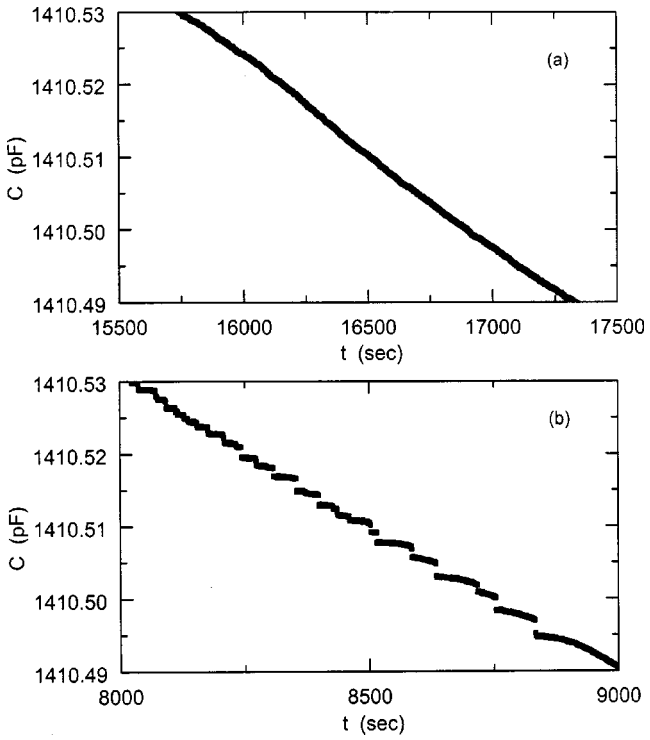

FIG. 20. Using a ^{3}He-^{4}He mixture (a) suppresses the avalanche behavior on a 30-nm sample. Compare the smooth draining in (a) for the mixture to approximately the same filling fraction region when pure ^{4}He is used (b). We have estimated the average density in our mixture to be 1.6% lower than for the case of pure ^{4}He. While the estimate for the mixture density involves some uncertainty, we clearly observe no jumps in capacitance in *any* region of the mixture run (a).

no detectable avalanches. For comparison, the same filling fraction range clearly had steps in the capacitance when pure ^{4}He was used [Fig. 20(b)]. The addition of the large amount of ^{3}He into the system clearly affected the avalanching behavior. A more complete study of this result should detail how the avalanches change for various concentrations of ^{3}He. Unfortunately, there were a number of problems that prevented us from pursuing a carefully controlled mixture study. As noted earlier, one problem was accurately knowing the mixture concentration as draining occurred. Since a simple pumping procedure was used to remove helium from the sample cell, the concentration of ^{3}He in the sample cell changed continuously with time. Clearly, one would like to maintain the concentration constant during a draining process. In our case the technique we used was designed for use with pure ^{4}He, not mixtures, and prevented the maintenance of constant concentration. We could not determine the absolute concentration to high reliability, although we could readily monitor concentration changes as helium removal occurred. The method used to measure the concentration for this experiment was to monitor the velocity of first (ordinary) sound, a compression wave in the vapor. The third-sound detector had adequate sensitivity to do this. The first-sound velocity u is given by

$$u^2 = \frac{\gamma k_B T}{m}, \tag{13}$$

where γ is the ratio of the specific heats, T the temperature, and m the mass of the atoms that compose the vapor. For a mixture of ^{3}He and ^{4}He,

$$m = \chi m_3 + (1-\chi) m_4, \tag{14}$$

where χ is the concentration of ^{3}He. Since the velocity only depends on the effective isotopic mass (and not on the pressure), the concentration of the vapor can be determined[35] by comparing the time of flight of an ordinary sound pulse in ^{4}He vapor, τ_4, to the time of flight of a pulse in the mixture vapor, τ_χ, by

$$\chi = \frac{m_4}{m_4 - m_3}\left(1 - \frac{\tau_\chi}{\tau_4}\right). \tag{15}$$

Using Eq. (13), the predicted velocity in ^{4}He (using $\gamma = 5/3$) is 7145 cm/sec. For pure ^{4}He we measure $\tau_4 = 67.60$ μsec, for a distance of 0.51 cm, and the resulting velocity is 7551 cm/sec. Defining τ from the ordinary sound pulses was not precise due to the noise in the case of such weak signals. For $\tau_A = 66.01$ μsec and $\tau_C = 66.23$ μsec, we calculated $\chi_A = 0.19$ and $\chi_C = 0.17$, where χ_A was the concentration in the gas after the first add, χ_C the concentration in the gas after the avalanches were finished, and $\tau_4 = 67.60$ μsec.

To estimate the concentration in the film for a given concentration in the gas, we use the measurements of Ellis *et al.*[35] They found that for concentrations of ^{3}He-^{4}He mixtures in a vapor of 0.168 and 0.277, the respective film concentrations were 0.06 and 0.12. We conclude that during the avalanche run, the mixture concentration in the film was $\chi_f \approx 0.06$, or possibly larger between B and C if the mixture was not removed uniformly. The presence of this dilute mixture was enough to remove or greatly suppress avalanche effects. At this concentration, a ^{3}He-^{4}He mixture remains superfluid, but the superfluid density is reduced. Measurements of the normal fluid fraction in mixtures are reported by Sobolev and Eselson.[36] For pure ^{4}He, Sobolev and Eselson found $\rho_n/\rho = 0.095$ for $T = 1.458$ K. When a mixture of $\chi = 0.085$ was measured at $T = 1.465$ K the normal fraction was found to have increased to $\rho_n/\rho = 0.335$. Our ^{3}He-^{4}He mixture at $T = 1.476$ K and $\chi \approx 0.06$ should have an increased normal fraction, but smaller than the 0.335 for the 8.5% mixture measured by Sobolev and Eselson. Thus, we conclude that even modest additions of ^{3}He substantially suppress the avalanches, perhaps more so than would be expected on the basis of simple superfluid density considerations.

VI. SUMMARY OF RESULTS FOR SINGLE-CAPACITOR MEASUREMENTS

We have presented data indicating that pores drain in large groups in a coordinated event when ^{4}He is removed from Nuclepore. The statistics of the pore draining have been determined and 200-nm-pore-diameter Nuclepore is seen to differ substantially from 30-nm-pore-diameter Nulcepore in its behavior. The steps in C as a function of t observed for both substrates only prove that groups of pores drain in a coordinated event and that they drain abruptly. There is no direct information about the mechanism involved. A number of possibilities exist. If the pores had discrete increments of pore sizes, all very close together, we would expect to observe steps upon draining in a simple noninteracting Preisach system. For the data that we see, this would require a significantly inhomogeneous pore structure, and with the manufacturing process of Nuclepore (etching damage tracks), it is unlikely such discrete groupings of pore sizes exist. Another possible explanation for these avalanches is that temperature fluctuations cause fluctuation in the chemical potential, inducing pores to drain all at once rather than draining smoothly. We do measure temperature fluctuations, but on a much longer time scale than we see avalanches. We are left to consider two important features of the system. First, the pores in Nuclepore are connected internally in a very complicated way. There are many intersections, and the porous structure is percolated. We also know from the hysteresis results[6] that pore coupling does exist. Second, we are using *superfluid* ^{4}He as the working fluid in these studies. The mobility of superfluid films is probably very important when 10^7 pores are draining in ~ 1 sec. The only way to remove this ^{4}He is either by film flow, by pipe flow, by evaporation, or by a combination of these. In addition to the mobility, surface sound modes such as third sound propagate on these films and bulk modes such as second and/or fourth sound can propagate in the pore spaces. In a subsequent publication, we will describe experiments that use multiple-capacitor Nuclepore samples[8,7] constructed in an effort to learn about the size scale of the avalanches and the coupling mechanism among pores. We have also done comparison experiments between Nuclepore and Anopore samples.[37] In Anopore pore intersections are nearly nonexistent. We will conclude that the superfluid film provides a relevant pore-pore coupling mechanism.

ACKNOWLEDGMENTS

We have benefited from and appreciate conversations with R.A. Guyer. This work was supported by the National Science Foundation through Grant Nos. DMR 94-22208, DMR 97-29805, and DMR 98-19122 and by Research Trust Funds provided by the University of Massachusetts, Amherst.

*Present address: Sandia National Laboratories, Albuquerque, NM 87185.

[1] D. H. Everett, in *The Solid-Gas Interface*, edited by E. A. Flood (Marcel Dekker, New York, 1967), Vol. 2, Chap. 36, p. 1055.

[2] Nuclepore is manufactured by Corning Inc., Acton, MA.

[3] D. T. Smith, J. M. Valles,Jr., and R. B Hallock, Phys. Rev. Lett. **54**, 1528 (1985).

[4] K. M. Godshalk and R. B. Hallock, Phys. Rev. B **36**, 8294 (1987).

[5] M. P. Lilly, P. T. Finley, and R. B. Hallock, Phys. Rev. Lett. **71**, 4186 (1993).

[6] M. P. Lilly and R. B. Hallock, Phys. Rev. B **63**, 17 450 (2001).

[7] M. P. Lilly and R. B. Hallock, Phys. Rev. B (to be published).
[8] M. P. Lilly, A. H. Wootters, and R. B. Hallock, Phys. Rev. Lett. **77**, 4222 (1996).
[9] D. T. Smith, K. M. Godshalk, and R. B. Hallock, Phys. Rev. B **36**, 202 (1987).
[10] K. R. Atkins, Phys. Rev. **113**, 962 (1959).
[11] Lakeshore calibrated germanium thermometer, model GR-200A-100.
[12] W. E. Keller, *Helium 3 and Helium 4* (Plenum Press, New York, 1969), p. 40.
[13] J. D. Jackson, *Classical Electrodynamics* (Wiley, New York, 1975).
[14] Andeen-Hagerling, Cleveland, OH, model 2500A.
[15] D. J. Bergman, Phys. Rev. **188**, 370 (1969).
[16] D. J. Bergman, Phys. Rev. A **3**, 2058 (1971).
[17] S. J. Putterman, *Superfluid Hydrodynamics* (North-Holland, Amsterdam, 1974).
[18] J. H. Sholtz, E. O. McLean, and I. Rudnick, Phys. Rev. Lett. **32**, 147 (1974).
[19] A variety of physical systems show power law behavior in distributions related to $D(s)$: sand in a rotating cylinder, H. M. Jaeger, C. Liu, and S. R. Nagel, Phys. Rev. Lett. **62**, 40 (1989); power law in a power spectrum, G. A. Held *et al.*, *ibid.* **65**, 1120 (1990); slip-stick friction, H. J. S. Feder and J. Feder, *ibid.* **66**, 2669 (1991); Barkhausen noise, P. J. Cote and L. V. Meisel, *ibid.* **67**, 1334 (1991); L. V. Meisel and P. J. Cote, Phys. Rev. B **46**, 10 822 (1992); J. S. Urbach, R. C. Madison, and J. T. Markert, Phys. Rev. Lett. **75**, 276 (1995); the motion of pinned vortices, S. Field, J. Witt, F. Nori, and X. S. Ling, *ibid.* **74**, 1206 (1995); martensites, E. Vives *et al.*, *ibid.* **72**, 1694 (1994); Hg porosimetry, A. H. Thompson, A. J. Katz, and R. A. Raschke, *ibid.* **58**, 29 (1987); acoustic emission (hydrogen precipitation in niobium), G. Cannelli, R. Cantelli, and F. Cordero, *ibid.* **70**, 3923 (1993); and magnetic domains in garnet films, K. L. Babcock and R. M. Westervelt, *ibid.* **64**, 2168 (1990).
[20] P. Bak, C. Tang, and K. Weisenfeld, Phys. Rev. Lett. **59**, 381 (1987); Phys. Rev. A **38**, 364 (1988).
[21] J. P. Sethna, K. Dahmen, J. A. Krumhansl, B. W. Roberts, and J. D. Shore, Phys. Rev. Lett. **70**, 3347 (1993).
[22] O. Perkovic, K. Dahmen, and J. P. Sethna, Phys. Rev. Lett. **75**, 4528 (1995).
[23] F. Preisach, Z. Phys. **94**, 277 (1935).
[24] R. A. Guyer and K. R. McCall, Phys. Rev. B **54**, 18 (1996).
[25] R. A. Guyer (private communication).
[26] R. A. Guyer and K. R. McCall, J. Low Temp. Phys. **111**, 841 (1998).
[27] The impedance was increased from $Z=5\times10^{9}$ cm^{-3} to $Z=1.5\times10^{10}$ cm^{-3} by inserting 10 cm of 0.028 cm SS wire into a 30 cm length of a 0.033-cm-i.d. capillary.
[28] S. Wang, K. S. Ketola, P. Lemaire, and R. B. Hallock, J. Low Temp. Phys. **119**, 645 (2000), and references therein.
[29] The above discussions presume that the fluid that drains from the Nuclepore pores is removed from the substrate system by evaporation or film flow and does not inhibit the draining. Calculations suggest that this should be the case.
[30] In this case the impedance was $Z=5\times10^{9}$ cm^{-3}.
[31] See, for example, D. S. Betts, *Refrigeration and Thermometry Below One Kelvin* (Sussex University Press, Sussex, 1976), pp. 173–176.
[32] M. P. Lilly and R. B. Hallock, J. Low Temp. Phys. **110**, 555 (1998).
[33] R. J. Donnelly, *Experimental Superfluidity* (University of Chicago Press, Chicago, 1967).
[34] J. C. Noiray, D. Sornette, J. P. Romagnan, and J. P. Laheurte, Phys. Rev. Lett. **53**, 2421 (1984).
[35] F. M. Ellis, J. S. Brooks, and R. B. Hallock, J. Low Temp. Phys. **56**, 69 (1984).
[36] V. Sobolev and B. Eselson, Zh. Éksp. Teor. Fiz. **60**, 240 (1971) [Sov. Phys. JETP **33**, 132 (1971)].
[37] A. H. Wootters, M. P. Lilly, and R. B. Hallock, J. Low Temp. Phys. **110**, 561 (1998).